Modeling of the Two-Phase Closed Thermosyphon

J. G. Reed[1]
Research Assistant.
Assoc. Mem. ASME

C. L. Tien
Professor.
Fellow ASME

Department of Mechanical Engineering,
University of California,
Berkeley, CA 94720

A comprehensive model is developed to predict the steady-state and transient performance of the two-phase closed thermosyphon. One-dimensional governing equations for the liquid and vapor phases are developed using available correlations to specify the shear stress and heat transfer coefficients. Steady-state solutions agree well with thermosyphon flooding data from several sources and with film thickness data obtained in the present investigation. While no data are available with which to compare the transient analysis, the results indicate that, for most systems, the governing time scale for system transients is the film residence time, which is typically much longer than the times required for viscous and thermal diffusion through the film. The proposed model offers a versatile and comprehensive analysis tool which is relatively simple.

Introduction

The two-phase closed thermosyphon, which is essentially a gravity-assisted, wickless heat pipe, utilizes the evaporation and condensation of an internal working fluid to transport heat, as shown in Fig. 1. The thermosyphon has been used in a variety of applications taking advantage of its high effective thermal conductivity or its thermal-diode property (the heat input must be in the lower portion of the device to achieve high effective thermal conductivity) [1]. When the thermosyphon is in stable operation, the internal flow is an annular, countercurrent, two-phase flow providing a convenient experimental facility for studying the features of such flows [2]. On the other hand, various fluid flow and heat transfer phenomena which can preclude stable, countercurrent, annular flow may occur. Examples of such flow limiting phenomena are the dryout, burnout (or film-boiling), and flooding limits which have been observed and described by many investigators [2–6].

Reflux condensation and countercurrent, annular, two-phase flows have been studied extensively in the recent past, largely because of their importance in nuclear reactor thermal-hydraulics [6–8]. Because of the many complex physical processes associated with reflux condensation and the nonlinearity of the governing equations, most analytical studies have focused attention on isolated phenomena, such as interfacial waviness. Little attention has been given to incorporating the results into comprehensive system models. This work attempts to overcome this deficiency by using a control-volume formulation which includes many complex physical phenomena, such as the augmentation of interfacial shear stress by film waviness, through empirical relationships, while maintaining the relative simplicity of the mathematical formulation.

The present formulation, similar to but more extensive than that first proposed by Dobran [3], models the thermosyphon directly from first principles and is applicable to either steady-state or transient operation of the device. The approach used here is very powerful because it provides a single system model which can predict most operating parameters and operating limits. Solutions for both steady-state and transient operation of the thermosyphon will be presented in this work. The predictions of the steady-state analysis will be compared with experimental data on film thickness obtained in the present study and with flooding data from the present study and from two other groups of investigators [4, 9]. The flooding predictions will also be compared with the predictions of the existing Tien–Chung correlation [5].

Analytical Model

It will be assumed throughout this analysis that terms of order $(\delta/R)^2$ and ρ_v/ρ_l are negligible relative to unity; that the vapor temperature is constant and the vapor is saturated; and that compressibility effects in the gas phase are negligible. These assumptions are well justified in most systems exhibiting countercurrent, annular flow in tubes [10–12]. This model also neglects entrainment of liquid droplets in the vapor core because this effect is usually insignificant except near the flooding limit.

In the formulation presented below, the thermosyphon is divided into seven control volumes. The liquid film, which is annular in cross section, and the vapor core, which is cylindrical in shape, are each divided into three control volumes,

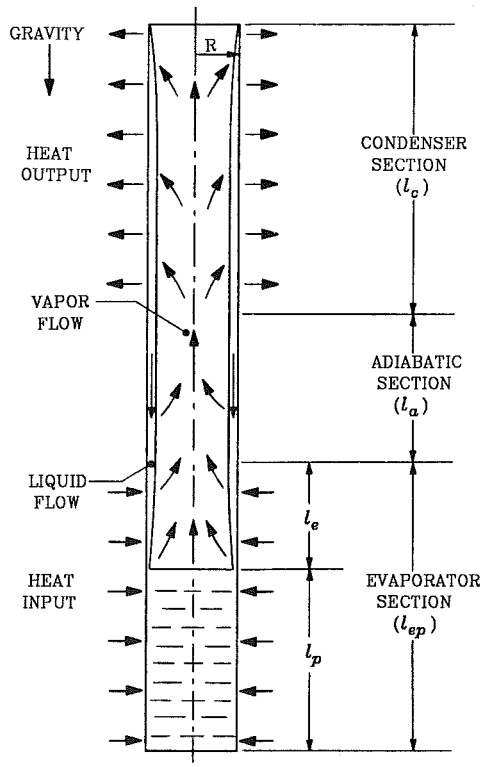

Fig. 1 A two-phase closed thermosyphon

[1]Present address: General Research Corporation, 5383 Hollister Ave., Santa Barbara, CA.

Contributed by the Heat Transfer Division for publication in the JOURNAL OF HEAT TRANSFER. Manuscript received by the Heat Transfer Division November 22, 1985.

one for each section of the device. The final control volume encloses the liquid pool at the bottom of the evaporator. The contribution to the convective flux terms at the top of the liquid pool caused by the motion of the control-volume boundary will be neglected because the assumptions of small δ/R and ρ_v/ρ_l imply that the rate of change of pool depth is small compared to the velocities of both the liquid film and the vapor.

In the following equations, the subscript k will be used to represent an arbitrary section of the thermosyphon and j the next section above it (or the top of the thermosyphon). In the equations using these subscripts, the different versions (a, b, and c) of the equations are obtained by setting $\langle k,j\rangle$ equal to $\langle c,t\rangle$, $\langle a,c\rangle$, and $\langle e,a\rangle$, respectively. If a subscript indicating one of the sections of the thermosyphon appears on a variable which is not an average value for the indicated section, the location to which the subscript refers is the bottom of the section (i.e., the interface with the next lower section).

Equations for the mass, momentum, and energy balances for each section of the liquid film are, respectively:

$$\frac{d}{dt}\left[l_k\rho_l\bar{\delta}_k\left(1-\frac{\bar{\delta}_k}{2R}\right)\right]=\dot{m}_k''l_k\left(1-\frac{\bar{\delta}_k}{R}\right)+\Gamma_j-\Gamma_k \quad (1a,b,c)$$

$$\bar{\delta}_k\left(1-\frac{\bar{\delta}_k}{2R}\right)[\rho_l g l_k-(P_k-P_j)]-l_k\left[\tau_{wk}+\left(1-\frac{\bar{\delta}_k}{R}\right)\tau_{ik}\right]$$
$$=\frac{d}{dt}(l_k\bar{\Gamma}_k)-u_{ik}\dot{m}_k''\left(1-\frac{\bar{\delta}_k}{R}\right)l_k+B_{l_k}\frac{{\Gamma_k}^2}{\delta_k\rho_l}\left(1+\frac{\delta_k}{2R}\right)$$
$$-B_{l_j}\frac{{\Gamma_j}^2}{\delta_j\rho_l}\left(1+\frac{\delta_j}{2R}\right) \quad (2a,b,c)$$

$$\frac{d}{dt}\left[\Delta\bar{T}_kC_p\rho_l\bar{\delta}_k\left(1-\frac{\bar{\delta}_k}{2R}\right)l_k\right]=l_k\left[\left(1-\frac{\bar{\delta}_k}{R}\right)\dot{m}_k''h_g-q_k\right]$$
$$+C_p\Delta T_j\Gamma_j-C_p\Delta T_k\Gamma_k \quad (3a,b,c)$$

Mass and momentum balances for the vapor core are of the form

$$\pi R^2\frac{d}{dt}\left[\rho_v\left(1-\frac{2\bar{\delta}_k}{R}\right)l_k\right]$$
$$=\dot{m}_k-\dot{m}_j-\dot{m}_k''2\pi R\left(1-\frac{\bar{\delta}_k}{R}\right)l_k \quad (4a,b,c)$$

$$\pi R^2\left(1-\frac{2\bar{\delta}_k}{R}\right)[l_kg\rho_v-(P_k-P_j)]+2\pi R\left(1-\frac{\bar{\delta}_k}{R}\right)l_k\tau_{ik}$$
$$=-\frac{d}{dt}(\bar{m}_kl_k)+u_{ik}\dot{m}_a''2\pi R\left(1-\frac{\bar{\delta}_k}{R}\right)l_k$$
$$-B_{vj}\frac{\dot{m}_j^2(1+2\delta_j/R)}{\pi R^2\rho_v}+B_{vk}\frac{\dot{m}_k^2(1+2\delta_k/R)}{\pi R^2\rho_v} \quad (5a,b,c)$$

The system of governing equations is completed by writing equations for the overall conservation of mass in the system and for energy balances on the liquid pool and the vapor core. The respective expressions are

$$M=\pi R^2\rho_l\left[l-\left(1-\frac{2\bar{\delta}_e}{R}\right)l_e-\left(1-\frac{2\bar{\delta}_a}{R}\right)l_a-\left(1-\frac{2\bar{\delta}_c}{R}\right)l_c\right] \quad (6)$$

$$\frac{d}{dt}\{\rho_vh_g[\pi R^2(l_c+l_a+l_e)-2\pi R(l_c\bar{\delta}_c+l_a\bar{\delta}_a+l_e\bar{\delta}_e)\}$$
$$=\rho_vh_g\left\{2\pi R\left[\dot{m}_e''l_e\left(1-\frac{\bar{\delta}_e}{2R}\right)-\dot{m}_a''l_a\left(1-\frac{\bar{\delta}_a}{2R}\right)\right.\right.$$
$$\left.\left.-\dot{m}_c''l_c\left(1-\frac{\bar{\delta}_c}{2R}\right)\right]+\dot{m}_e\right\} \quad (7)$$

$$\pi R^2\frac{d}{dt}[\rho_lC_p\Delta\bar{T}_pl_p]=2\pi R\left[q_el_p-\frac{\dot{m}_e}{2\pi R}h_g+\Gamma_eC_p\Delta T_e\right] \quad (8)$$

In addition to these basic governing equations, auxiliary equations specifying the wall and interfacial shear stresses and the liquid-film heat transfer coefficient are needed. The expressions to be used are listed in Table 1. The turbulent-vapor interfacial friction factor is a recently obtained correlation [13] while the other expressions can be found in textbooks [10–12]. The interfacial friction factor for laminar vapor flow contains a correlation factor as suggested by Blangetti and Naushahi accounting for the influence of interfacial mass flux [14]. For turbulent vapor flow, the effect of interfacial waviness dominates the effect of interfacial mass transfer so the mass transfer effect is not included. Several different values for the film Reynolds number at the transition to turbulent flow, ranging from 1200 to 2400, have been used by various investigators [10–12]. The transition from laminar to turbulent film flow will be assumed here to begin at a

Nomenclature

$B_{\varphi j}$ = ratio of the average squared velocity to the average velocity squared for phase φ at the location specified by subscript j (velocity profile shape factor)
Bo = Bond number $=(4\rho_lgR/\sigma)^{1/2}$
C_f = friction factor defined by $\tau=\frac{1}{2}\rho_lu^2C_f$
C_p = liquid specific heat evaluated at the liquid bulk temperature
g = gravitational acceleration
Gr = two-phase Grashof number $=(8gR^3/\nu_l^2)^{1/2}$
h = liquid film heat transfer coefficient defined by $q=h(T_v-T_w)$
h_g = vapor phase enthalpy $=h_{fg}+C_p(T_v-T_w)$
h_{fg} = latent heat of vaporization evaluated at T_v
Ja = Jakob number $=C_p\Delta T_N/h_{fg}$
k_l = liquid thermal conductivity evaluated at the liquid bulk temperature
l = overall length of the thermosyphon
l_j = length of thermosyphon section indicated by subscript j
$\dot{m}_j''$ = average mass flux due to phase change at the liquid–vapor interface in the thermosyphon section indicated by subscript j
$\dot{m}_j$ = upward mass flow rate of vapor at the location specified by subscript j
P_j = pressure at location j
Pr = liquid Prandtl number $=\mu_lC_p/k_l$
q_j = wall heat flux in section j
Q_e = total heat input in evaporator
R = tube inside radius
Re_φ = Reynolds number of phase φ, $4\Gamma/\mu_l$ for the liquid film, and $2\dot{m}/(\pi R\mu_v)$ or $\mathrm{Re}_l\mu_l/\mu_v$ for the gas core
T_j = bulk temperature of liquid at location j or vapor temperature if $j=v$ (temperature differences are relative to T_w)
t = time
u = streamwise (axial) velocity
x_1, x_2 = parameters used in shear

Table 1 Shear stress and heat transfer coefficient expressions for use in control-volume equations

Quantity	Expression
Wall shear, laminar film	$\tau_w = \mu_l \left(\frac{du}{dy}\right)_w$, from velocity profile
Wall friction factor, turbulent film	$C_f = 0.079\mathrm{Re}^{-1/4}$ (Blasius relation)
Interfacial friction factor, laminar vapor core	$C_f = (16./\mathrm{Re})[\varphi/(e^{\varphi}-1)]$ $\varphi = \dot{m}'' R/(4\mu_v)$
Interfacial friction factor, turbulent vapor core	$C_f = 0.005 + x_1(\delta/R)^{x_2}$ where $x_1 = 0.2574(\mathrm{Bo}/2)^{x_2} 10^{9.07/\mathrm{Bo}}$, $x_2 = 1.63 + 4.74/\mathrm{Bo}$
Film heat transfer coefficient, laminar film	$h = k_l/\delta$
Film heat transfer coefficient, turbulent film	$h = 0.056\mathrm{Re}^{-1/5}\mathrm{Pr}^{1/3} k_l/(\nu_l^2/g)^{1/3}$

Reynolds number of 2040, the point at which the laminar and turbulent wall shear stress expressions match in the absence of interfacial shear. When interfacial shear stress is present, the laminar and turbulent expressions are smoothed together over the Reynolds number range 2040 to 3500.

In addition to predicting the values of various system variables such as film thicknesses in the various sections of the device, mass fluxes, liquid pool depth, and vapor temperature, the present analysis can be used to predict the dryout and flooding operating limits. Dryout phenomena can be predicted by the present model in two ways: (1) The depth of the liquid pool may become equal to zero indicating that the supply of working fluid is insufficient for a complete flow circuit; (2) the value of Γ_e may become equal to zero which means that there is no flow of liquid reaching the liquid pool. In the steady-state case, within the framework of this model, the two types of dryout are essentially the same and the two limits will be reached simultaneously. However, in the transient case, the film may dry out above the liquid pool if the evaporator heat flux is increased rapidly; so, in general, the pool-dryout and film-dryout limits are distinct. When any portion of the evaporator tube wall becomes dry, there is a drastic loss of cooling efficiency and therefore a danger of severe overheating. The flooding, or entrainment, limit is predicted when the calculated rate of change of film thickness with respect to heat input becomes unbounded in some section of the device [8]. Physically, a vertical slope on a film thickness versus heat input curve means that an increase in flow rate will increase the interfacial shear stress too much to be balanced by the corresponding increase in the weight of the liquid film. The result is a net upward force on the liquid film which will retard the downward flow of liquid and a transition to a complicated, nonannular flow regime or an oscillatory flow pattern.

Steady-State Operation

In this section, consideration will be given to situations in which the thermosyphon is in steady-state operation with the evaporator heat flux and condenser wall temperature having constant specified values. In addition to the assumptions made in the general formulation, it will be assumed in the present case that δ/R and Ja/Pr are small relative to unity and that Ja is less than the order of unity. These assumptions are not very restrictive in most cases. Countercurrent annular flow has not been observed for δ/R greater than 0.1 [10], and the restrictions on Ja and Ja/Pr are met by most common working

Nomenclature (cont.)

stress correlation defined in Table 1
α_l = liquid film thermal diffusivity $= k_l/(\rho_l C_p)$
Γ_j = mass flow rate in the liquid film per unit tube perimeter at the location specified by subscript j
δ_j = film thickness at location specified by subscript j
Δ = difference or increment
ϵ_j = dimensionless film thickness in section j
ϑ = dimensionless temperature
μ_φ = dynamic viscosity of phase φ
ν_φ = kinematic viscosity of phase φ
ρ_φ = density of phase φ
σ = liquid surface tension (evaluated at T_v)
τ_{kj} = shear stress on surface k in thermosyphon section j

Subscripts

a = adiabatic section
c = condenser section
e = portion of evaporator above the liquid pool where there is film flow
ep = complete evaporator section including both the liquid pool and film flow regions
i = phase interface
f = final steady state following a transient
l = liquid phase
N = Nusselt solution
p = liquid pool
r = ramp input function for transient analysis
t = top of the thermosyphon
v = vapor phase
w = tube wall
0 = initial state in transient analysis

Superscripts

$\dot{}$ = per unit time
$''$ = per unit area
$\bar{}$ = axially averaged over a given section of the thermosyphon (this designation is omitted if a variable is axially averaged by definition)
$*$ = nondimensional variable

fluids because flooding usually occurs before the heat input is large enough for Ja to exceed unity. It will also be assumed that the dynamic pressure of the vapor, $\rho_v u_v^2$, is small relative to the static pressure head of the liquid film, $\rho_l g l_c$. This is equivalent to the requirement that $(\Gamma^*/\mathrm{Gr})^2 R^*/\rho^*$ be much less than unity. This condition is generally satisfied unless the tube radius is very small or the vapor density is very low. In all cases considered in this study, the above dimensionless group is of the order 0.01 or less. The newly introduced assumptions imply that the temperature profile in the liquid film in the condenser can be well approximated as linear when the film is laminar (i.e., $h = k_l/\delta$) [15] and that, in the liquid-film momentum equations, the pressure drop, interfacial-momentum-flux, and inertia terms are negligible [7, 16].

In thermophysical property calculations and energy convection terms, the bulk temperature of the liquid in the condenser will be taken as the average of the vapor and wall temperatures. In the adiabatic section and the evaporator, it will be assumed that the liquid is at the vapor temperature.

The following variables are introduced for use in nondimensionalizing the steady-state governing equations:

$$q_j^* = \frac{l_j q_j}{\mu_l h_{fg}}, \quad \Gamma_j^* = \frac{\Gamma_j}{\mu_l}, \quad \epsilon_j = \frac{\delta_j}{R},$$

$$\dot{m}_j^* = \frac{\dot{m}_j}{2\pi R \mu_l}, \quad \dot{m}_j''^* = \frac{\dot{m}_j'' l_j}{\mu_l}, \quad M^* = \frac{M}{\pi R^2 l \rho_l},$$

$$\vartheta_j = \frac{\Delta T_j}{\Delta T_N}, \quad \tau_j^* = \frac{\tau_j}{g\rho_l \delta_N}, \quad l_j^* = \frac{l_j}{l},$$

$$R^* = \frac{R}{l}, \quad \rho^* = \frac{\rho_v}{\rho_l}, \quad \mu^* = \frac{\mu_l}{\mu_v} \tag{9a}$$

where

$$\Delta T_N = \left(\frac{q_e l_{ep}}{0.943 l_c}\right)^{4/3} \left[\frac{l_c \nu_l}{g\rho_l h_{fg} k_l^3}\right]^{1/3}$$

and

$$\delta_N = \left[4 \frac{\mathrm{Ja}}{\mathrm{Pr}} \frac{\nu_l^2 l_c}{g}\right]^{1/4} \tag{9b}$$

The definitions in equations (9*b*) are based on the Nusselt solution [11] for laminar condensation on a plate of length l_c with a temperature drop across the film calculated to give the same total heat transfer per unit width as the specified heat input per unit perimeter in the evaporator.

The dimensionless system of steady-state governing equations resulting from introduction of the above variables and the simplifications discussed above is

Mass balances:

$$\dot{m}_k''^* = \Gamma_k^* - \Gamma_j^* \tag{10a, b, c}$$

$$\dot{m}_k''^* - \dot{m}_k^* - \dot{m}_j^* \tag{11a,b,c}$$

$$M^* = 1 - (1 - 2\epsilon_e) l_e^* - (1 - 2\epsilon_a) l_a^* - (1 - 2\epsilon_c) l_c^* \tag{12}$$

Energy balances:

$$\dot{m}_k''^* (1 + \mathrm{Ja}\vartheta_v) = q_k^* l_k + \Gamma_j^* \mathrm{Ja}\vartheta_j - \Gamma_k^* \mathrm{Ja}\vartheta_k \tag{13a,b,c}$$

$$\dot{m}_e^* (1 + \mathrm{Ja}\vartheta_v) = q_e^* l_p^* + \Gamma_e^* Ja\vartheta_e \tag{14}$$

Force balances:

$$\epsilon_k/\epsilon_N = \tau_{wk}^* + \tau_{ik}^* \tag{15a,b,c}$$

Any one of the energy equations, (13*a–c*) or (14), can be replaced by the simpler steady-state system energy balance given by

$$q_c^* l_c^* = q_e^* l_{ep}^* \tag{16}$$

Due to the simplifications in the liquid-film momentum equations, it is not necessary to solve the vapor-core momentum equations simultaneously with the rest of the system. The coupling of the liquid and vapor momentum equations is in the interfacial shear stress, interfacial momentum flux, and pressure drop terms, but in the simplified system, only the vapor flow rate and density are needed, together with the interfacial friction factor, to specify the interfacial shear. The vapor flow rates are obtained in terms of the liquid flow rates by substituting the interfacial mass transfer rates found in equations (10*a, b, c*) into equations (11*a, b, c*). The resulting equations simply state that, under steady-state conditions, the downward mass flow rate of liquid is equal to the upward mass flow rate of vapor at any cross section of the device.

When the film flow is laminar, a differential force balance on the liquid film, of the type used in Nusselt's analysis but including interfacial shear, predicts a parabolic velocity profile in the film. Using this result and the friction factors defined in Table 1, the wall shear stress expressions to be used in equations (15*a, b, c*) for laminar and turbulent films respectively are

$$\tau_{wj}^* = \frac{\tau_{ij}^*}{2} + \frac{24 A_{wj} \bar{\Gamma}_j^*}{\mathrm{Gr}^2 \epsilon_N \epsilon_j^2} \tag{17a}$$

$$\tau_{wj}^* = \frac{0.223 A_{ij} (\bar{\Gamma}_j^*)^{7/4}}{\mathrm{Gr}^2 \epsilon_N \epsilon_j^2} \tag{17b}$$

and the respective interfacial shear stress expressions for laminar and turbulent vapor flow are

$$\tau_{ij}^* = \frac{64 A_{ij} \bar{\Gamma}_j^* [1 + \rho^*/(2\epsilon_j)]}{\mathrm{Gr}^2 \epsilon_N (\rho^*/\mu^*)} \tag{17c}$$

$$\tau_{ij}^* = \frac{16 A_{ij} (\bar{\Gamma}_j^*)^2 [1 + \rho^*/(2\epsilon_j)]^2 (0.005 + x_1 \epsilon_j^{x_2})}{\mathrm{Gr}^2 \epsilon_N \rho^*} \tag{17d}$$

The coefficients A_{wj} and A_{ij} are weight factors accounting for the fact that the average interfacial shear stress in a given section of the device may differ from the product of the average friction factor and the average dynamic pressure. The factors will be approximated by assuming the following: In the condenser, the film thickness and flow rate are given by the Nusselt solution; in the adiabatic section, the film thickness and flow rate are constant; and in the evaporator, the flow rate varies linearly down the tube (because q_e is constant) and the film thickness is constant. Using these assumptions, and the equality of liquid and vapor flow rates, the axial variation of the shear stresses can be estimated and estimates of A_{wj} and A_{ij} obtained.

The interfacial shear stress expressions given above are based on the velocity of the vapor relative to average velocity of the liquid film. The factor $[1 + \rho^*/(2\epsilon_j)]$, seen in equations (17*c*) and (17*d*), represents the ratio of the relative vapor velocity to the absolute vapor velocity. This factor differs considerably from unity under some circumstances.

The system of equations is solved by using the mass and energy equations, (10)–(14), together with the shear stress expressions, equations (17*a–d*), to express all variables in terms of: ϵ_c, ϵ_a, ϵ_e; the specified system geometry and fill quantity; the specified boundary conditions, T_w and q_e; and the thermophysical properties of the working fluid (which are known functions of temperature). The result is a set of three nonlinear, algebraic equations for ϵ_c, ϵ_a, and ϵ_e. The equation for ϵ_c is not coupled to the other two, and the equation for ϵ_a is independent of ϵ_e so the three equations can be solved successively by numerical techniques.

Experimental Study

To assess the accuracy of the analytical model proposed, experimental data have been obtained using a two-phase closed thermosyphon which has been used in previous work [7] but

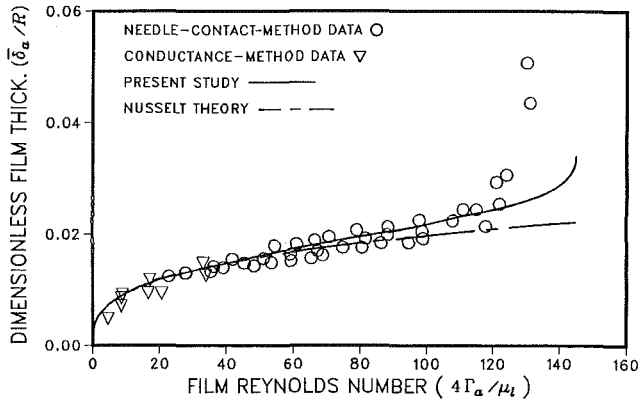

Fig. 2 Experimental data and theoretical predictions from the present study for adiabatic-section film thickness (working fluid is methanol, $R = 0.71$ cm, $l_c = 1.08$ m, $l_a = 0.305$ m, $l_{ep} = 1.03$ m, $T_w = 36°C$)

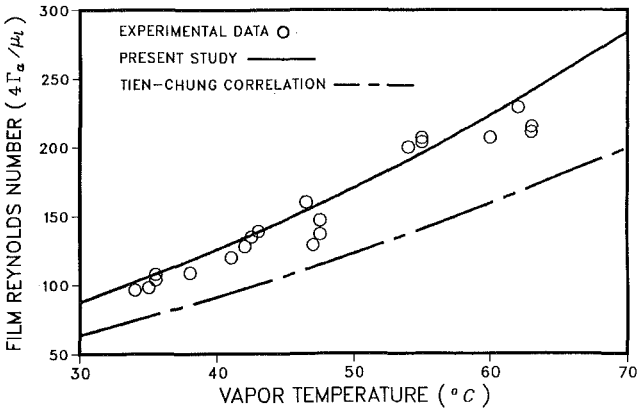

Fig. 3 Experimental data and theoretical flooding predictions from the present study (working fluid is methanol, same device as Fig. 2)

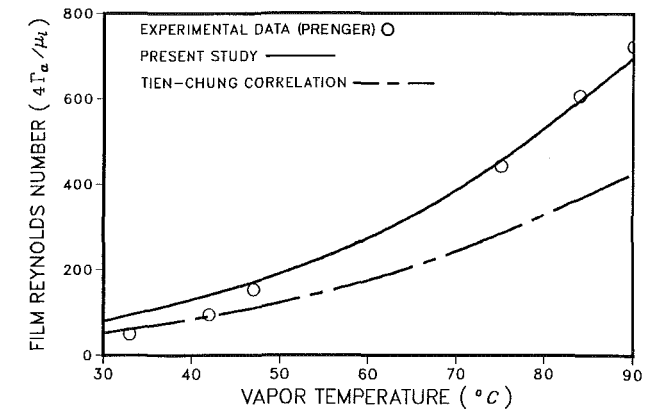

Fig. 4 Experimental data of Prenger [9] and theoretical flooding predictions from the present study (working fluid is water, $R = 1.03$ cm, $l_c = 1.26$ m, $l_a = 1.0$ cm, $l_{ep} = 55.9$ cm)

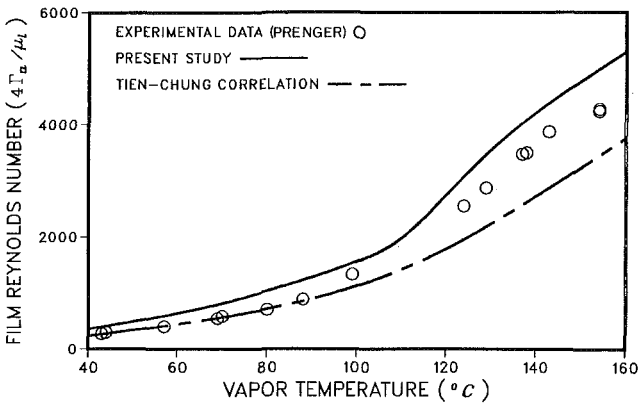

Fig. 5 Experimental data of Prenger [9] and theoretical flooding predictions from the present study (working fluid is methanol, same device as Fig. 4)

which has been modified to include several transparent flow observation sections in the condenser and adiabatic sections. A detailed description of the apparatus and experimental procedures can be found in a supporting document for this paper [16].

Results and Comparison With Experimental Data

The steady-state system of equations has been solved over a range of operating temperatures and heat inputs for several different thermosyphon geometries and two different working fluids chosen to correspond to conditions represented by the experimental data to be presented. Flooding data from the present study and from two other groups of investigators and film thickness data from the present study will be presented [4, 9].

Figure 2 shows the dependence of film thickness in the adiabatic section on the film Reynolds number (essentially evaporator heat input) as predicted by the analysis of the present study and by Nusselt theory, which neglects interfacial shear stress. Corresponding film-thickness data, obtained with the apparatus of the present study using the film-conductance and needle-contact methods, are also presented. The theoretical curves assume a condenser wall temperature of 36°C which is representative of the conditions displayed in the experimental data (the range of condenser inside-wall temperatures represented in the data is approximately 34°C to 38°C, depending on heat input). The agreement between the predictions of the present study and the experimental data is seen to be quite good although the experimental data indicate flooding slightly before the rapid up-turn in the theoretical curve which occurs at $Re_f \approx 145$. For reference, it is noted that

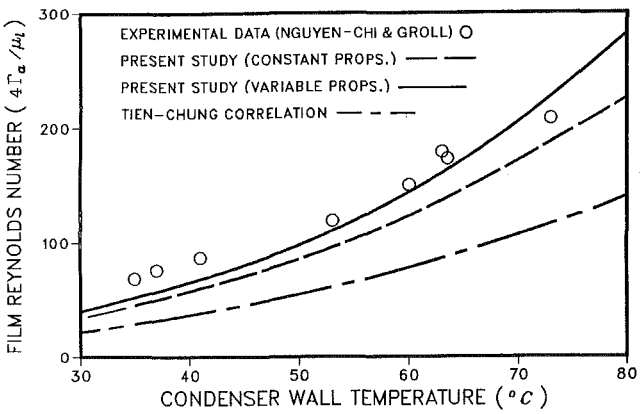

Fig. 6 Experimental data of Nguyen-Chi and Groll [4] and theoretical flooding predictions from the present study (working fluid is water, $R = 0.850$ cm, $l_c = 1.00$ m, $l_a = 50.0$ cm, $l_{ep} = 1.00$ m)

the predicted film Reynolds numbers at flooding corresponding to condenser wall temperatures of 34°C and 38°C are 135 and 156, respectively.

As expected, the film-thickness predictions are very close to those of Nusselt theory for low Reynolds numbers and become progressively greater than those predicted by Nusselt theory as the film Reynolds number, and therefore the interfacial shear stress, increases. The qualitative features of the film thickness versus Reynolds number curves predicted by the present analysis will be similar to the curve shown in Fig. 2 for other working fluids and temperature ranges. However, the

Reynolds number required for flooding and the rapidity of the increase of film thickness with the Reynolds number will depend significantly on the thermophysical properties of the working fluid, particularly through variations in the values of Gr and ρ^*.

Figures 3–6 present experimental flooding data along with the corresponding analytical predictions. Each figure plots the film Reynolds number at flooding versus the working fluid vapor temperature or condenser wall temperature (depending on which temperature was measured in the corresponding experimental investigation). If both the wall temperature and the vapor temperature were measured, the data are presented on the basis of the vapor temperature because the flooding point tends to be more sensitive to the vapor temperature than to the wall temperature. The flooding curve predicted by the commonly used, semi-empirical, Tien–Chung correlation is also presented in each figure for comparison with the current analysis. The Tien–Chung correlation predicts flooding when

$$\left(4\frac{\Gamma_a^*}{\mathrm{Gr}}\right)^{1/2}[1+(\rho^*)^{-1/2}]=\frac{1.79}{\mathrm{Bo}^{1/4}}\tanh(0.5\mathrm{Bo}^{1/2}) \tag{18}$$

From the methanol flooding data of the present study shown in Fig. 3, it can be seen that the present analysis predicts the data very well. On the other hand, while the Tien–Chung correlation correctly predicts the trend of the data, the flooding points tend to be predicted prematurely. The tendency of the Tien–Chung correlation to underpredict thermosyphon flooding data is seen in all of the data sets presented here. This may be a result of the fact that many of the experimental studies from which the constant factor in the correlation was derived used experimental facilities in which test-section entrance effects are significant. In a thermosyphon, the tube is continuous, so entrance effects are eliminated.

Figure 4 shows data collected at Los Alamos National Laboratory (LANL) using water as the working fluid [9]. The device used to obtain the data did not have an adiabatic section but a 1-cm adiabatic section is assumed for calculational purposes. As in the first data set, the present analysis shows good agreement with the data while the Tien–Chung curve lies below the data. The data appear to show a greater increase with temperature of the Reynolds number at flooding than that predicted by either the present analysis or by the Tien–Chung correlation. However, there are not enough data points to judge whether or not this is significant.

Figure 5 presents LANL flooding data for methanol [9]. The agreement between the predictions of the present analysis and the data is quite good. Although the predicted results are slightly above the experimental data, the present analytical model predicts the change in curvature of the flooding curve resulting from the transition to turbulent film flow. This effect is not reflected in the predictions of the Tien–Chung correlation, and the predictions of the correlation fall considerably below the data at the high end of the temperature range. It is interesting to note that, under the conditions represented by the data, the liquid velocity is of the same order of magnitude as the vapor velocity and, near the upper end of the temperature range, the vapor velocity is only about twice as large as that of the liquid. If the absolute vapor velocity, rather than the velocity relative to the liquid film, is used for calculating the interfacial shear stresses, the predictions of the current analysis are as much as 55 percent above the experimental data.

Figure 6 presents thermosyphon flooding data for water reported on the basis of thermosyphon wall temperature [4]. In the constant-property solution, all physical properties are evaluated at the wall temperature while in the variable property solution the properties are evaluated at the local bulk liquid temperature based on the calculated vapor temperature. The data presented are from a thermosyphon operating at an inclination angle of 10 deg from vertical, the closest case to vertical operation for which data were reported. It can be seen that all of the theoretical curves underpredict the heat input at flooding. However, it can be estimated, from data on the effect of thermosyphon inclination on flooding [4], that the heat input at flooding for a vertical thermosyphon, using water as the working fluid, will be below that for a thermosyphon inclined 10 deg from vertical by about 25 percent at a condenser wall temperature of 30°C and by about 5 percent at a wall temperature of 60°C. The agreement between the experimental data and the theoretical predictions of this analysis is very good if the effect of inclination angle is considered.

When all of the flooding and film thickness data are considered, the predictions of the proposed model are seen to be very good. This is significant because it shows that many aspects of the behavior of the thermosyphon can be accurately modeled within a single comprehensive model based on a first-principle analysis. This approach has a sounder basis and is more versatile than analyses relying on simple scaling laws and correlations.

Transient Operation

This section analyzes the transient operation of the two-phase closed thermosyphon. The particular situation considered here is the commonly occurring case of laminar flow of the liquid film accompanied by turbulent flow in the vapor core. In many practical situations, the thermosyphon wall temperature or heat flux will vary with time. This analysis considers the evolution in time of the thermosyphon operating characteristics in response to a time varying heat input in the evaporator with the condenser wall temperature maintained at a constant value. The results are useful in determining the conditions under which the device operation can be treated as a sequence of quasi-steady states and those under which a complete transient calculation is required. The simplicity of the control-volume approach is of great value in the transient analysis because the inclusion of time dependence in the governing equations causes a much less dramatic increase in the complexity of the computations required to obtain numerical solutions than that which would result if a differential formulation were used.

The simplifying assumptions used in the steady-state analysis will also be used here. In addition, the variation of liquid properties with temperature will be neglected. The use of the steady-state shear stress and heat transfer coefficients in the transient analysis implies the assumption that the temperature and velocity profiles respond to transients over time scales much shorter than those characterizing the overall system response. The validity of this assumption is treated in detail elsewhere [16], but it is also justified on the basis of the results of the analysis.

As in the steady-state analysis, the superheat required for boiling or evaporation will be neglected. One consequence of neglecting the details of the boiling phenomena in the evaporator is that the distribution of the heat input to the liquid pool between evaporation of the liquid in the pool and changing its temperature is indeterminate. In the present analysis, it will be assumed that the liquid pool is always at the same temperature as the vapor (i.e., saturated liquid state) unless the vapor temperature is increasing too rapidly for the heat input in the liquid pool to provide the necessary energy to meet this condition. When the condition of equality of liquid pool and vapor temperatures cannot be satisfied, the evaporative mass flux in the pool is set equal to zero and all of the heat input in the liquid pool is assumed to be in the form of sensible heat.

The variables which will be used for nondimensionalizing the governing equations are the same as those used in the steady-state analysis. In the transient analysis the

characteristic temperature difference will be taken as ΔT_0, the initial temperature drop across the liquid film, and the characteristic film thickness is the corresponding film thickness calculated from Nusselt theory [15]. In addition to the previously defined variables, a dimensionless time variable is introduced

$$t^* = t\left(\frac{g\delta_N^2}{3\nu_l l_c}\right) \tag{19}$$

The time scale used here is based on a characteristic film residence time obtained using the film thickness and mass flow rate predicted by the Nusselt theory for a plate of length l_c and a temperature difference of ΔT_0. The film residence time is chosen because the transient evolution of the system is controlled by the film residence time and the condensation rate rather than, for example, the thermal diffusion time of the liquid film.

The system of dimensionless governing equations for transient operation of the thermosyphon, with the introduction of the previously discussed simplifications, is given below. Mass balances for the liquid film, vapor core, and total system, respectively, are

$$\frac{l_j^*}{\epsilon_N}\frac{d\epsilon_j}{dt^*} = \dot{m}_j''^* - \Gamma_j^* + \Gamma_k^* \tag{20a, b, c}$$

$$\frac{l_j}{2\epsilon_N}\frac{d\rho^*}{dt^*} = \dot{m}_j' - \dot{m}_j''^* - \dot{m}_k''^* \tag{21a, b, c}$$

$$M^* = 1 - (1-2\epsilon_e)l_e^* - (1-2\epsilon_a)l_a^* - (1-2\epsilon_c)l_c^* \tag{22}$$

Energy balances for the liquid film and the liquid pool are

$$\mathrm{Ja}\frac{l_j^*}{\epsilon_N}\left(\epsilon_j\frac{d\vartheta_v}{dt^*} + \vartheta_v\frac{d\epsilon_j}{dt^*}\right) = q_j^* l_j^* + \Gamma_k^*\mathrm{Ja}\vartheta_k - \Gamma_j^*\mathrm{Ja}\vartheta_j - \dot{m}_j''^*(1+\mathrm{Ja}\vartheta_v) \tag{23a, b, c}$$

$$\mathrm{Ja}\frac{l_p^*}{\epsilon_N}\frac{d\vartheta_p}{dt^*} = q_e^* l_p^* + \Gamma_e^*\mathrm{Ja}\vartheta_v - \dot{m}_e^*(1+\mathrm{Ja}\vartheta_v) \tag{24}$$

The liquid-film momentum balances are

$$\frac{\epsilon_j}{\epsilon_N} = \tau_{wj}^* + \tau_{ij}^* \tag{25a, b, c}$$

As in the steady-state analysis, the vapor-core momentum equations are omitted because they are decoupled from the rest of the system through the simplifications used in the liquid-film momentum equations. Also note that, because the vapor is assumed saturated, there is no vapor-phase energy equation.

The details of the numerical solution procedure will be omitted for brevity as they are documented elsewhere [16]. In essence, the system can be reduced to a set of four first-order differential equations in time, coupled to ten nonlinear algebraic equations which are used to estimate the values of the time derivatives for stepping the solution out in time. The time integration is performed using a Runge–Kutta technique [17].

Results of Transient Analysis

Solutions of the system of transient governing equations have been carried out for several representative cases to illustrate the type of results obtained from the present model. Figures 7–9 show the response of various system variables to several different transient evaporator heat flux inputs for a thermosyphon using water as the working fluid with the geometry and initial operating state summarized in Table 2.

Figure 7 shows the system response to ramp increases in evaporator heat flux of two different rise times, $\Delta t_r^* = 0.118$ (1.00 s) and $\Delta t_r^* = 2.35$ (20.0 s). The response curve for each variable is plotted in a normalized form as the ratio of the difference between the current and initial values of a variable and

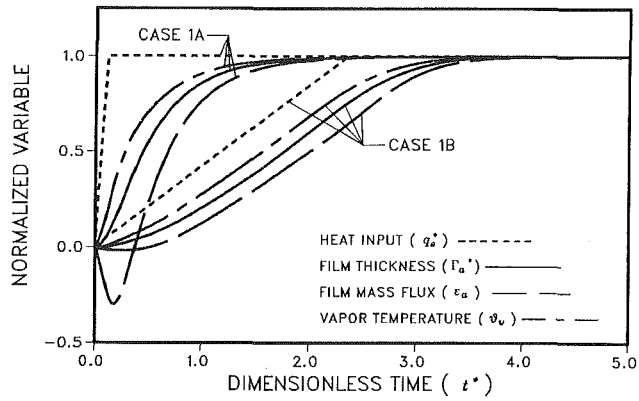

Fig. 7 Transient responses of vapor temperature, film thickness in the adiabatic section, and liquid mass flux in the adiabatic section to ramp increases in evaporator heat flux

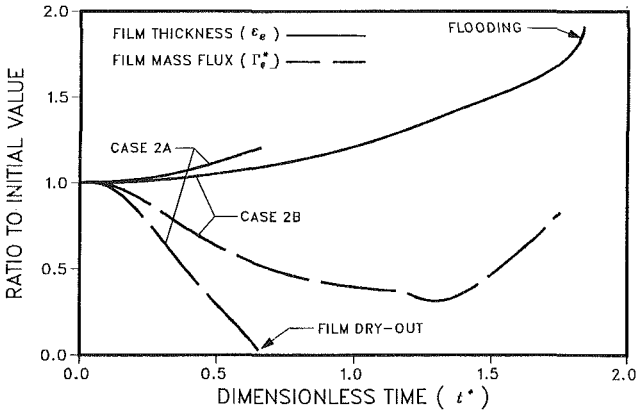

Fig. 8 Flooding and evaporator film dryout under transient conditions

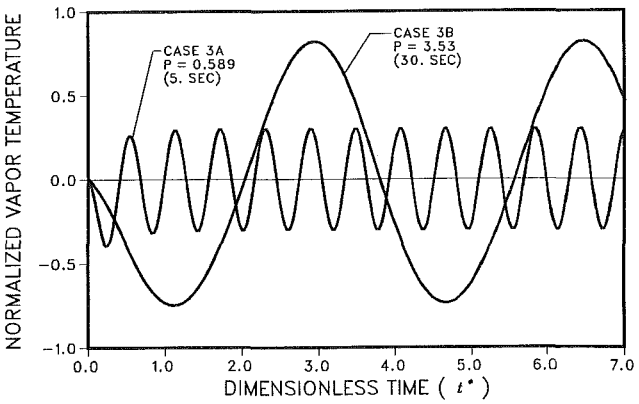

Fig. 9 Response of vapor temperature to sinusoidal variations in evaporator heat input of two different frequencies

the difference between the steady-state values at the beginning and end of the transient. The final values of the variables displayed in Fig. 1 are: $\epsilon_{a_f} = 0.0178$, $\Gamma_{af}^* = 42.8$, and $\vartheta_{v_f} = 1.53$. The dimensionless time variable t^* can be converted to dimensional form (in units of seconds) by multiplying by 8.50. The initial and final values of q_e^* are 32.9 and 42.7 which correspond to approximately 70 percent and 90 percent, respectively, of the value required for flooding. For reference, it is noted that the increases in ϵ_a, Γ_a^*, and ϑ_v displayed in Fig. 7 correspond to 22 percent, 30 percent, and 47 percent of their respective initial values.

The transient response curves in Fig. 7 illustrate several points. First, the vapor temperature response leads the

Table 2 Initial thermosyphon operating state for transient calculations (working fluid is methanol, $T_w = 60.0°C$, $R = 1.0$ cm, $l_c = 1.0$ m, $l_a = 0.25$ m, $l_{ep} = 1.0$ m)

Variable	Value	Variable	Value	Variable	Value
Γ_c^*	32.7	Γ_a^*	32.9	Γ_e^*	13.4
ϵ_c	1.01×10^{-2}	ϵ_a	1.44×10^{-2}	ϵ_e	1.20×10^{-2}
ϑ_v	1.04	M^*	0.100	Bo	24.1
Gr	6.17×10^{4}	Ja	9.02×10^{-3}	ρ^*	1.68×10^{-4}

Table 3 Influence of variation of dimensionless parameters on rise times of selected system variables ($t = 8.5t^*$)

	t_{50}^*			t_{90}^*		
	ϑ_v	ϵ_a	Γ_a^*	φ_v	ϵ_a	Γ_a^*
Case 1A	0.282	0.448	0.681	0.956	1.14	1.35
$M^* \rightarrow 1.5M^*$	0.381	0.558	0.791	1.25	1.45	1.66
$\rho^* \rightarrow 2\rho^*$	0.259	0.433	0.574	0.877	1.04	1.16
Ja→2Ja	0.471	0.645	0.865	1.55	1.74	1.94
Bo→Bo/2	0.264	0.436	0.595	0.879	1.06	1.21
Gr→2Gr	0.139	0.300	0.371	0.596	0.664	0.691

responses of the fluid dynamic variables, ϵ_a and Γ_a^*. This is expected because the temperature difference between the condenser wall and the vapor core provides the driving force for condensation. Second, the dimensionless time required for the system to re-establish steady-state operation, after the transient in heat input, is of the order of unity, verifying that the film residence time is the controlling time scale for the transient evolution of the system. If the dimensionless time scale had been based on film thickness and thermal diffusivity of the liquid, the rise time for the system would be of the order of 10^3 dimensionless time units. Lastly, the convergence of the rise times of the heat input function and the system response between Case 1A with a rapid rise in heat flux and Case 1B, with the heat flux increasing over a period of time comparable to the natural rise time for the system, indicates that for variations of evaporator heat flux with characteristic rise times or periods of oscillation substantially greater than $t^* = 1$, the system response should be well approximated by a sequence of steady-state calculations.

To provide an indication of the influence of the various dimensionless parameters on system response, calculations with the same condenser wall temperature and transient heat-input function as Case 1A of Fig. 7 have been performed with modified values for various parameters as summarized in Table 3. The parameters t_{50}^* and t_{90}^* displayed in Table 3 are the dimensionless rise times required for the indicated system variable to reach 50 percent and 90 percent of its normalized final value. The results displayed in the table indicate that the system response tends to become more rapid if the Grashof number or density ratio is increased or if the Bond number is decreased, and the system response is slowed if the Jakob number or fill quantity is increased. The decreases in system response time caused by increasing Gr, increasing ρ^*, or decreasing Bo can be explained by the fact that each of these changes tends to reduce the film residence time and, thus, speed the response of the system. Reducing Bo or increasing ρ^* will cause a reduction in the interfacial shear stress while an increase in Gr will cause a reduction in wall shear. All of these effects tend to increase the velocity of the film. The slower response times associated with an increased value of M^* or Ja reflect the increase in thermal capacitance of the liquid pool resulting from these changes.

Figure 8 illustrates the progress of the system toward the flooding and film dryout operating limits under transient conditions. The initial operating state is that summarized in Table 2. The variables are normalized by their initial values. In contrast to the cases shown in Fig. 7, the final value of evaporator heat flux is $q_e^* = 51.6$ which is 10 percent above the value required for flooding as predicted by the steady-state analysis. In Case 2A, with a rapid increase in evaporator heat flux, Γ_e, the film mass flux entering the liquid pool becomes equal to zero at $t^* \approx 0.7$ ($t \approx 6$ s) indicating dryout of the liquid film in the evaporator. This case is interesting because dryout would not be predicted by a steady-state calculation. It should be noted that, although in the example case presented the heat flux in the evaporator is above that required for flooding, this is not a necessary condition for dryout of the film. In fact, dryout of the liquid film in the evaporator during a transient increase in evaporator heat flux can be predicted at heat flux values substantially below those required for flooding. The key criterion for this limit is that the time scale for changes in film thickness and mass flux be long compared to the rise time of the change in heat flux. In situations where this criterion is satisfied, dryout of the film would be expected if

$$q_e^* > \frac{\Gamma_e^*}{l_e^*} \tag{26}$$

where the right-hand side is evaluated at the start of the transient. The criterion discussed above also assumes that the mass of the film is small enough that the time required to evaporate the film is small compared to the film residence time.

In Case 2B, the rate of increase of q_e^* is small enough that film dryout is avoided. However, because the heat input exceeds the value required for flooding, the increase in film thickness in the adiabatic section becomes unbounded at $t^* \approx 2.0$. The evaporator mass flux also increases rapidly near the flooding limit but this is believed to be a numerical effect caused by the rapid increase in film thickness. The change in slope of evaporator mass flux at $t^* \approx 1.2$ is caused by the end of the ramp increase in heat flux. The lag in response of ϵ_a indicates that the system can operate in an un-flooded state at values of heat input above the steady-state flooding limit if the duration of the heat flux transient is sufficiently short.

Figure 9 shows the response of system vapor temperature to sinusoidal variations in evaporator heat flux of two different frequencies. The initial operating state is, as before, the one summarized in Table 2. The two heat-flux input functions have the form

$$q_e^* = 32.9 - 9.80\sin(2\pi t^*/p) \quad (27)$$

where p is the period of the input and the amplitude has been chosen so that the peak is the same as the final heat input value of Fig. 7. Figure 9 plots the difference between the current vapor temperature and the initial vapor temperature, normalized by the difference between the steady-state vapor temperature corresponding to the peak of the sinusoidal heat input and the initial vapor temperature. Two points are illustrated in the figure. First, the response curves are slightly asymmetric about the t^* axis. This is to be expected because of the nonlinearity of the governing equations. Second, when the period of the input is small relative to the characteristic rise time of the system, the amplitude of the response is greatly attenuated. On the other hand, if the period of the input is of the same order or greater than the rise time of the system, the response can probably be well approximated as a sequence of steady states.

In order to assess the accuracy of the calculations presented above, it is desirable to compare the results of the analysis with experimental data. Unfortunately, attempts to obtain experimental data on the transient operation of the system used in this study have proven to be unsuccessful because of thermal masses in the system not reflected in the model, and no data are available in the literature. Thus, although the results of the transient analysis are consistent with expected system behavior, quantitative assessment of its accuracy will require a specially designed experiment or an expansion of the model to include the thermal masses of the thermosyphon components.

Conclusions

A first-principle formulation of the governing equations for steady-state and transient operation of the two-phase closed thermosyphon has been solved for several representative cases. The steady-state predictions agree well with available experimental data. The ability of the model to predict the transient response of the system and to predict operating limits under transient conditions has been demonstrated, although experimental data with which to compare the predictions are currently unavailable. The results of the analysis indicate that, in the parameter regime considered, the most important time scale controlling the transient response of the system is the film residence time (or runoff time). On this basis, it can be concluded that steady-state analysis of the thermosyphon will be valid as long as transient inputs to the system have characteristic time constants (or periods of oscillation) which are long compared to the film residence time. The proposed model provides a powerful and versatile analytical model of the two-phase closed thermosyphon while maintaining a relatively simple mathematical formulation.

Acknowledgments

The support of this work by the Electric Power Research Institute under grant EPRI RP 1160-3 is gratefully acknowledged.

References

1 Dunn, P., and Reay, D. A., *Heat Pipes*, 3rd ed., Pergamon Press, New York, 1982.

2 Fukano, T., Chen, S. J., and Tien, C. L., "Operating Limits of the Closed Two-Phase Thermosyphon," *Proc. ASME/JSME Thermal Eng. Conf.*, Vol. 1, 1983, pp. 95–101.

3 Dobran, F., "Steady-State Characteristics and Stability Thresholds of a Closed Two-Phase Thermosyphon," *Int. J. Heat Mass Transfer*, Vol. 28, 1985, pp. 949–957.

4 Nguyen-Chi, H., and Groll, M., "Entrainment or Flooding Limit in a Closed Two-Phase Thermosyphon," *Advances in Heat Pipe Technology*, D. A. Reay, ed., Pergamon Press, New York, 1981, pp. 147–162.

5 Tien, C. L., and Chung, K. S., "Entrainment Limits in Heat Pipes," *AIAA Journal*, Vol. 17, 1981, pp. 643–646.

6 Calia, C., and Griffith, P., "Modes of Circulation in an Inverted U-Tube Array With Condensation," *Thermal-Hydraulics in Nuclear Power Technology*, ASME-HTD, Vol. 15, New York, 1981, pp. 35–43.

7 Chen, S. J., Reed, J. G., and Tien, C. L., "Reflux Condensation in a Two-Phase Closed Thermosyphon," *Int. J. Heat Mass Transfer*, Vol. 27, 1984, pp. 1587–1594.

8 Seban, R. H., and Faghri, A., "Condensation in a Vertical Tube With a Closed Top," *Int. J. Heat Mass Transfer*, Vol. 27, 1984, pp. 944–948.

9 Prenger, F. C., Los Alamos National Laboratory, Los Alamos, New Mexico, private communication, 1984.

10 Wallis, G. B., *One Dimensional Two-Phase Flow*, McGraw-Hill, New York, 1969, Ch. 11.

11 Collier, J. G., *Convective Boiling and Condensation*, 2nd ed., McGraw-Hill, New York, 1981, Ch. 10.

12 Hewitt, G. F., and Hall-Taylor, N. S., *Annular Two-Phase Flow*, Pergamon Press, New York, 1970.

13 Bharathan, D., Wallis, G. B., and Richter, H. J., *Air-Water Counter-Current Annular Flow*, EPRI Report NP-1165, 1979.

14 Blangetti, F., and Naushahi, M., "Influence of Mass Transfer on the Momentum Transfer in Condensation and Evaporation Phenomena," *Int. J. Heat Mass Transfer*, Vol. 23, 1980, pp. 1694–1695.

15 Rohsenow, W. M., "Heat Transfer and Temperature Distribution in Laminar-Film Condensation," *Trans. ASME*, Vol. 83, 1961, pp. 1645–1648.

16 Reed, J. G., *Analytical Modeling of the Two-Phase Closed Thermosyphon*, Ph.D. Thesis, Department of Mechanical Engineering, University of California, Berkeley, CA, 1985.

17 Carnahan, B., Luther, H. A., and Wilkes, J. O., *Applied Numerical Methods*, Wiley, New York, 1969.